Shape Control and Characterization of Transition Metal Diselenides MSe_2 (M = Ni, Co, Fe) Prepared by a Solvothermal-Reduction Process

Jian Yang,[†,‡] Guang-Hui Cheng,[†] Jing-Hui Zeng,[†] Shu-Hong Yu,*[,†,‡] Xian-Ming Liu,[‡] and Yi-Tai Qian*[,†,‡]

Department of Chemistry and Structural Research Laboratory, University of Science and Technology of China, Hefei, Anhui 230026, P. R. China

Received July 20, 2000. Revised Manuscript Received November 19, 2000

Transition metal diselenides (MSe_2, M=Ni, Co, Fe) were synthesized successfully through a simple solvothermal-reduction reaction at low temperatures. EDXA and XPS techniques confirmed that the compositions of these diselenides were in good agreement with their stoichiometries. With increasing temperature, the obtained $NiSe_2$ transformed from initial filament nanocrystallites to final octahedral crystals. The studies on the thermal stability of the as-prepared $NiSe_2$ showed that NiSe acted in an intermediate role in the pyrolysis process. The Raman spectrum of $NiSe_2$ presented the peak of the Se−Se stretching mode at 216.5 cm^{-1}. XRPD techniques revealed that the as-prepared $CoSe_2$ at higher temperature had an orthorhombic structure similar to that of $FeSe_2$. At low temperature this orthorhombic phase $CoSe_2$, which displayed rodlike shape with the growth direction along ⟨121⟩, coexisted with a trace of the cubic phase $CoSe_2$.

Introduction

The magnetic and electrical properties of many transition metal dichalcogenides have showed large varieties in behavior and have been studied in considerable detail.[1,2]Typical substances such as FeS_2, CoS_2, and NiS_2 are diamagnetic semiconductor, ferromagnetic metal, and antiferromagnetic semiconductor, respectively.[3] $CoSe_2$ is an exchange-enhanced Pauli paramagnet in its ground state, while at higher temperature it behaves as if it has local magnetic moments.[4] $NiSe_2$ is one of the typical Pauli paramagnets with metallic conductivity.[5] These stoichiometric compounds and the solid solutions between them now have been regarded as typical materials for studies of the physical characteristics associated with a narrow band electron system.[6] Meanwhile, transition metal dichalcogenides have extensive applications in energy areas such as electrochemistry and catalysis.[7] The large surface areas and high activity of nanomaterials will enhance their applications in these fields.

Usually, crystalline transition metal dichalcogenides are synthesized by the direct stoichiometric combination of elements in evacuated silica tubes.[8,9]But due to the limit of slow diffusion, the complete reaction requires intermittent grinding and heating at high temperature from 500 to 1200 °C. Parkin's group improved direct elemental reactions by conducting them in liquid ammonia at room temperature, but the obtained product was a mixture of amorphous nickel selenide and crystalline element Ni.[10] The mixture was heated at 300 °C and produced crystalline $NiSe_2$ and NiSe. Novel organometallic precursors also were used to prepare transition metal diselenides. Steigerwald and co-workers reported that the reaction between bis(cyclooctadiene) nickel and tri(ethylphosphine selenide) at 270 °C produced crystalline Ni_3Se_2 and elemental Ni that was difficult to be removed from the product.[11] Our group has successfully prepared a series of selenides via solvothermal processes. Wang synthesized one-dimen-

* Corresponding author. E-mail: shyu@ustc.edu.cn.
† Department of Chemistry.
‡ Structural Research Laboratory.

(1) Wold, A.; Dwight, K. In *Solid State Chemistry*; Chapman and Hall: New York, 1993; p 179.
(2) (a) Jarrett, H. S.; Cloud, W. H.; Bouchard, R. J.; Butler, S. R.; Frederick, C. G.; Gilson, G. L. *Phys. Rev. Lett.* **1968**, *21*, 617. (b) Marcus, S.; Bither, T. A. *Phys. Lett. A* **1970**, *32*, 363. (c) Panissod, P.; Krill, G.; Lahrichi, M.; Lapierre, M. F. *Phys. Lett. A* **1971**, *59*, 221.
(3) (a) Sato, K.; Takeda, M. *J. Phys. Soc. Jpn.* **1969**, *26*, 631. (b) Benoit, R. *J. Chem. Phys.* **1955**, *52*, 119. (c) Morris, B.; Johnson Wold, A. *J. Phys. Chem. Solids* **1967**, *28*, 1564.
(4) Noue, I.; Yasuoka, H. *Solid State Commun.* **1979**, *30*, 341.
(5) Noue, I.; Yasuoka, H.; Ogawa, S. *J. Phys. Soc. Jpn.* **1980**, *48* (3), 850.
(6) (a) Matsuura, A. Y.; Watamable, H.; Kim, C.; Doniach, S.; Shen, Z. X.; Thio, T.; Bennett, J. W. *Phys. Rev. B.* **1998**, *58* (7), 3690. (b) Otoro, R.; De Vidales, J. L. M.; De Las Heras, C. *J. Phys.: Condens. Matter.* **1998**, *10* (31), 6919. (c) Miyadai, T.; Saitoh, M.; Tazuke, Y. J. *J. Magn. Magn. Mater.* **1992**, *104/107*, 1953.
(7) (a) Jacobson, A. J.; Chianelli, R. R.; Whittingham, M. S. *J. Electrochem. Soc.* **1979**, *126*, 2277. (b) Dines, M. B. *J. Chem. Educ.* **1974**, *51*, 221. (c) Voorhoeve, R. J. H. *J. Catal.* **1979,** *23*, 236. (d) Voorhoeve, R. J. H.; Stuiver, J. C. *J. Catal.* **1971**, *23*, 243. (e) Baresel, D.; Sarholz, W.; Scharner, P.; Schmitz, J. *Ber. Bungsenges. Phys. Chem.* **1974**, *78* (6), 608.
(8) (a) Leith, R. M. A.; Terhell, J. C. *Transition Metal Dichalcogenides* In *Preparation and Crystal Growth of Materials with Layered Structures*; Leith, R. M. A., Ed.; D. Reidel: Dordrecht, The Netherlands, 1977**.** (b) Braveer, G. *Handbook of Preparative Inorganic Chemistry*, 2nd ed., Academic Press: New York, **1965**; Vols. 1 and 2.
(9) Wang, P.; Somasundaram, P.; Honig, J. M.; Pekarek, T. M. *Mater. Res. Bull.* **1997**, *32* (10), 1435.
(10) Henshaw, G.; Parkin, I. P.; Shaw, G. A. *J. Chem. Soc., Dalton Trans.* **1997**, 231.
(11) Brennan, J. G.; Siegrist, T.; Kwon, Y. U.; Stuczynski, S. M.; Steigerwald, M. L. *J. Am. Chem. Soc.* **1992**, *114*, 10334.

10.1021/cm0005945 CCC: $20.00
Published on Web 02/07/2001

Table 1. Synthetic Conditions of $NiSe_2$ and the Corresponding Results

sample	solvent	temp, °C	reaction time, h	morphology	av size
a	Py	80	12	filament	510 nm (width)
b	Py	120	12	irregular shape	25 nm
c	Py	180	12	irregular shape + octahedra	0.6 μm
d	Py	180	48	octahedra	1.5 μm
e	DMF	180	12	spherical	40 nm

sional monoselenides by the reaction of metal chlorides, KBH_4, and selenium in ethylenediamine.[12] Han studied the multiphase transitions among nickel selenides by the reaction between $NiC_2O_4{\cdot}2H_2O$ and elemental selenium.[13]

In this paper, a convenient route was developed for the preparation of transition metal diselenides (MSe_2, M=Ni, Co, Fe) at low temperature. The characterization of the products was reported with emphasis on $NiSe_2$ and $CoSe_2$. These diselenides were identified by EDXA, XPS, and XRPD techniques. The shape and size of $NiSe_2$ were well controlled by changing the synthetic conditions. The thermal stability of the as-prepared $NiSe_2$ was studied and a reasonable mechanism was proposed for the pyrolysis process. The XRPD pattern of the obtained $CoSe_2$ was indexed as the orthorhombic structure similar to that of $FeSe_2$. The observed values were in good agreement with the calculated ones. The effect of synthetic conditions on the phase and morphology of $CoSe_2$ nanoparticles was investigated.

Experimental Section

All reagents are analytical grade and are used without any further purification. Typically, elemental Se (~3.75 mmol) and powdered NaOH (~7.5 mmol) were put into a 50 mL conical flask that already had contained 25 mL of solvent such as distilled H_2O, *N*,*N*-dimethyl formamide (DMF), pyridine (Py), acetyl acetone (acac), and ethylenediamine (en). A small amount of hydrazine (~0.14 mL) was added into the solution under violent stirring. The solution was stirred for 3 h to ensure that the mixture would evenly disperse in the solution. After this, an appropriate amount of transition metal chlorides MCl_2 (M = Ni, Co, Fe) was added to the solution. Then the solution was stirred again for half an hour. Finally, the whole solution was poured into a Teflon-lined stainless autoclave. The autoclave was maintained at 80−200 °C for 12−48 h. After it was cooled to room-temperature naturally, the solution was filtered. The obtained precipitate was washed with distilled H_2O, absolute alcohol several times, and then dried in a vacuum at 60 °C for 1 h. The obtained powders were collected for characterization.

X-ray powder diffraction patterns (XRPD) were obtained on a Japan Rigaku D/Max-γA rotation anode X-ray diffractometer equipped with graphite monochromatized Cu Kα radiation (λ = 1.541 78 Å), employing a scanning rate of 0.02 deg s^{-1} in the 2θ range from 10° to 70°. Transmission electron microscope photographs (TEM), selected area electron diffraction (SAED), and energy-dispersive X-ray analysis (EDXA) were performed on a Hitachi model H-800 transmission electron microscope, using an accelerating voltage of 200 kV. The samples for these measurements were dispersed in absolute ethanol by vibration in an ultrasonic pool. Then the solutions were dropped onto Cu grids coated with amorphous carbon films. Scanning electron microscopic (SEM) photographs were taken from a Hitachi X-650 scanning electron microanalyzer. X-ray photoelectron spectra (XPS) were recorded on a VEGSCALAB MKII X-ray photoelectron spectrometer, using nonmonochromatized Mg Kα radiation as the excitation source. Thermogravimetric analysis (TG) was carried on a shimadzu TGA-50H thermogravimeter analyzer. Scans were run at a ramp rate of 10 °C/min from room temperature to 800 °C under nitrogen atmosphere. Typical sample sizes were 4−7 mg. The onset of decomposition was calculated on the basis of a default trigger value of 1% of the starting sample mass. The Raman spectrum was recorded on a SPEX-1403 Laser Raman Spectrometer by means of backscattering technique, ranging from 100 to 300 cm^{-1} at room temperature.

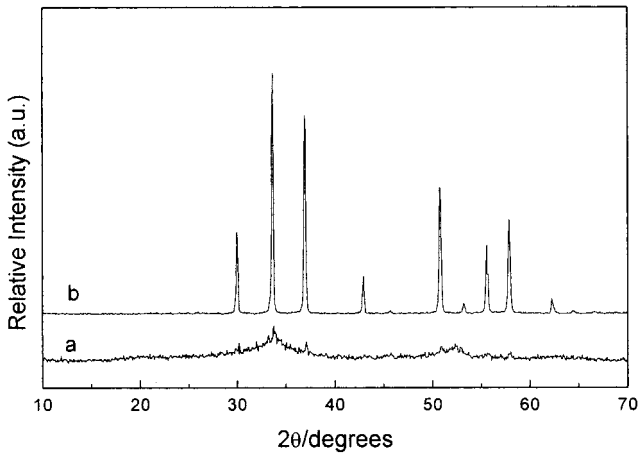

Figure 1. XRPD pattern of (a) sample a, (b) sample b.

Results and Discussion

Preparation and Characterization of $NiSe_2$. The different synthetic conditions of $NiSe_2$ and the corresponding results are summarized in Table 1. The XRD pattern of sample a, as shown in Figure 1a, consisted of two broad diffraction peaks, which indicated that the crystallinity of the sample was low. EDXA technique was used to determine the composition of the sample. It showed that only Ni and Se were present in the sample. The molar ratio of Ni:Se obtained from the peak areas was 34.5:65.5, which was consistent with the stoichoimetry of $NiSe_2$. If the reaction proceeded at 120 °C for 12 h, sample b was well crystallized and the XRPD pattern (Figure 1b) coincided well with the pure cubic phase $NiSe_2$ (penroseite). The lattice parameter calculated from the XRPD pattern was a = 5.96 Å, which was close to the reported data in the literature.[14] The crystal size calculated from the Debye−Scherrer equation was 20 nm.[15]

Besides Py, other organic solvents were also used to synthesize $NiSe_2$ at low temperature. The pure cubic phase $NiSe_2$ was prepared at 80 °C for 12 h in DMF. The aprotic character of DMF lead to the remarkable increase in activity of anionic species such as E_x^{2-}, which is responsible for the preparation of metal chalcogenides.[16] However, similar preparation in distilled

(12) Wang, W. Z.; Geng, Y.; Yan, P.; Liu, F. Y.; Xie, Y.; Qian, Y. T. *J. Am. Chem. Soc.* **1999**, *121*, 4062.
(13) Han, Z. H.; Yu, S. H.; Li, Y. P.; Zhao, H. Q.; Li, F. Q.; Xie, Y.; Qian, Y. T. *Chem. Mater.* **1999**, 11, 2302.
(14) JCPDS File, No. 41-1495.
(15) Klug, H. P.; Alexander, L. E. *X-ray Diffraction Procedures for Polycrystalline and Amorphous Materials*; Wiley: New York, 1962.

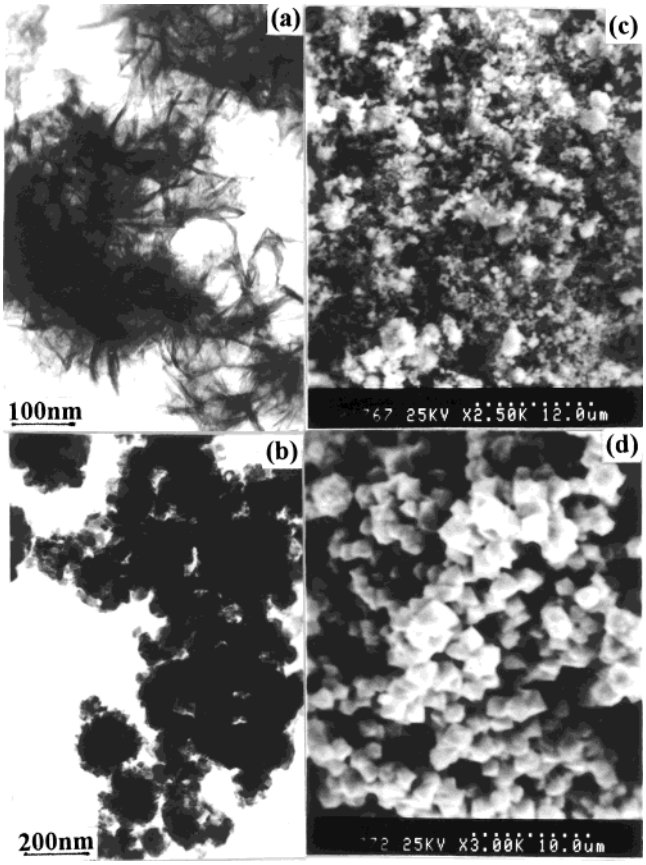

Figure 2. SEM and TEM photographs of different samples: (a) sample a, (b) sample b, (c) sample c, (d) sample d.

water, acetyl acetone, and ethylenediamine at the same temperature failed. Elemental selenium was often observed in the products obtained from distilled water and acetyl acetone. It is believed that the appearance of selenium in the products is relevant to the lower solubility of selenium in these solvents. In addition, the complexes of metal ion and solvents were found in the products obtained from acetyl acetone and ethylenediamine. This result indicates that these solvents with strong coordination ability do harm to the formation of diselenides at low temperature.

TEM and SEM photographs of the products under different reaction conditions are shown in Figure 2. Sample a consisted of agglomerated filaments 5−10 nm in width (Figure 2a). The electron diffraction pattern was composed of several diffused rings, which indicated that the product was poorly crystallized. When the temperature was increased up to 120 °C, only agglomerated irregular particles with an average size of about 25 nm were observed in sample b (Figure 2b). Even at 180 °C for 12 h, most of the obtained product still remained irregular in shape, although there was a trace of octahedra (Figure 2c). When the reaction time was prolonged to 48 h, the irregular particles completely became regular octahedra with an average size of about 1.5 μm (Figure 2d). The formation of octahedral crystals can be attributed to the effect of the crystal habit on the morphology.[13] The smaller nucleation rate, which can be obtained by reducing the alkality or changing the solvents, will favor the formation of regular octahedra. This conclusion has been confirmed by our experiments.

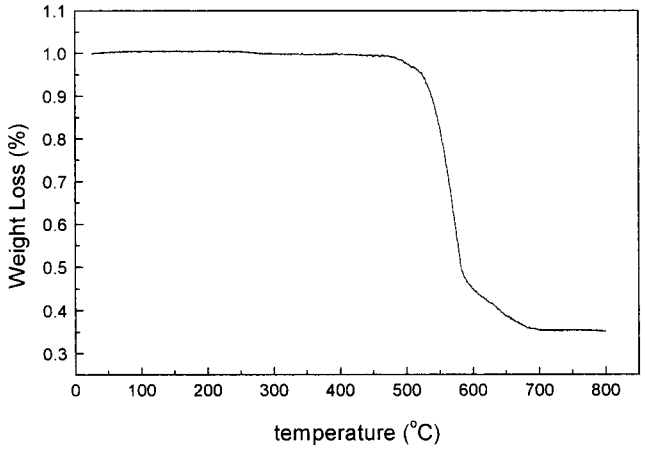

Figure 3. TG curve of $NiSe_2$ under N_2 atmosphere,

The different morphologies of the samples at different temperatures can be explained by reaction control and growth control. When the reaction was carried out at low temperature, the slow reaction rate lead to that the influence of the reaction on the product was dominant. In this case, the filament morphology observed in the product probably was relevant to that Se trended to form needle crystals in pyridine. With the increasing temperature, the reaction rate gradually increased.[17] The influence of the growth process on the morphology was observed. The shape of the product changed from filaments to irregular particles. At higher temperatures, since the reaction was completed in a short time, the product was in the growth process for most of the time (Ostwald ripening). Controlled by the crystal habit, the irregular particles grew to octahedral crystals at higher temperature.

The chemical composition of the product was determined by XPS technique. All binding energies were corrected for specimen charging by referencing the contaminated carbon 1s signal to 284.5 eV. The typical survey spectrum of $NiSe_2$ revealed the presence of nickel and selenium on the surface. High-resolution spectra were preformed at Ni and Se core regions. The binding energies of Ni2p3 at 853.10 eV and Se3d at 54.55 eV were in good agreement with the reported value in the literature.[18,19] The signals belonging to metal oxide and selenium oxide were not observed in the spectra. The presence of carbon and oxygen in the survey spectrum can be attributed to the absorption of gaseous molecules.[20] All these results confirmed the formation of nickel diselenide.

TG-DTG analysis was used to study the thermal stability of the as-prepared diselenides. TGA result of $NiSe_2$ at 10 °C/min from room temperature to 800 °C under N_2 atmosphere is shown in Figure 3. A smooth decomposition occurred at an onset temperature of

(16) (a) Sheldrick, W. S.; Wachhold, M. *Angew. Chem., Int. Ed. Engl.* **1997**, *36*, 206. (b) Dance, I.; Fisher, K. *Prog. Inorg. Chem.* **1994**, *41*, 637.

(17) Noggle, J. H. *Physical Chemistry*, 2nd ed.; Scott, Foresman and Company: Boston, 1989.

(18) Van der Heide, H.; Hermel, R.; Vanbruggen, C. F.; Haas, C. *J. Solid State Chem.* **1980**, *33*, 17.

(19) Wagner, C. D. *Handbook of X-ray photoelectron Spectroscopy*, Perkin-Elmer Corporation: Minnesota, 1979.

(20) Li, Y. D.; Liao, H. W.; Ding, Y.; Zhang Y.; Qian, Y. T. *Inorg. Chem.* **1999**, *38*, 1382.

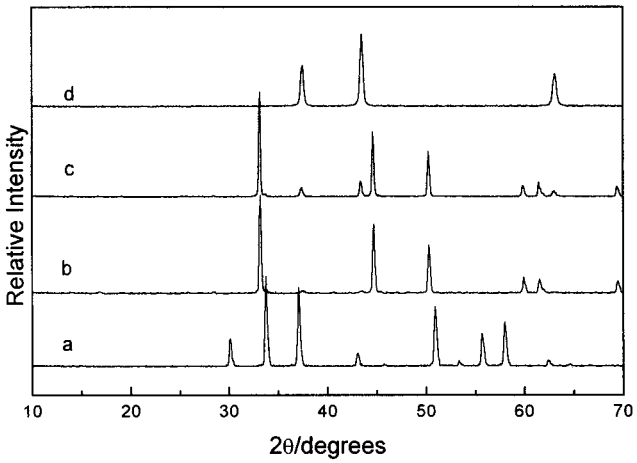

Figure 4. Pyrolysis products obtained by treating $NiSe_2$ at 650 °C for different times: (a) initial product, $NiSe_2$; (b) 2 h, NiSe +NiO; (c) 4 h, NiSe + NiO; (d) 6 h, NiO.

approximately 530.56 °C and a completion temperature of approximately 600.25 °C. The final decomposition product was confirmed to be NiO by XRPD technique. Moreover, the amount of 64.91% mass loss was in excellent agreement with the calculated value of 65.84% mass loss based on eq 1 for the production of NiO.

$$NiSe_2 + O_2 \Rightarrow NiO + Se \text{ or } SeO_2 \qquad (1)$$

According to the equation, the elemental ratio of Ni:Se was 1:1.93, which was close to the value from other techniques. However, the DTG curve displayed an asymmetric peak, which indicated that the decomposition of $NiSe_2$ probably was not a single-step process. To further study the decomposition process, the products which were obtained by treating $NiSe_2$ under N_2 atmosphere at 650 °C for different times were identified by XRPD technique (Figure 4). It was found that NiSe acted as an intermediate during the transition from $NiSe_2$ to NiO. Probably since the bond of Se−Se is weak, it can be cleaved easily at high temperature. So, $NiSe_2$ decomposed to produce NiSe at first, which then was oxidized to NiO. The whole process can be expressed as follows:

$$NiSe_2 \Rightarrow NiSe + Se \qquad (2)$$

$$NiSe + O_2 \Rightarrow NiO + SeO_2 \qquad (3)$$

The Raman allowed modes in the pyrite structure are mainly caused by the intraionic stretching modes of dumbbell shaped Se_2 units. The intraionic Se−Se stretching mode of pyrite-type compounds exhibits interesting insights into the strengths of the intraionic bonds. In the as-prepared $NiSe_2$, the peak of the Se−Se stretching mode was observed at 216.5 cm^{-1} (Figure 5), which was close to the value observed in other diselenides.[21−23] Although the as-prepared $CoSe_2$ and $FeSe_2$ own the same Se−Se unit, no pronounced peaks were observed in the range 100−300 cm^{-1}. This seems to be relevant to the crystal structure, because the as-prepared $CoSe_2$ and $FeSe_2$ are not the pyrite structure but the orthorhombic structure.

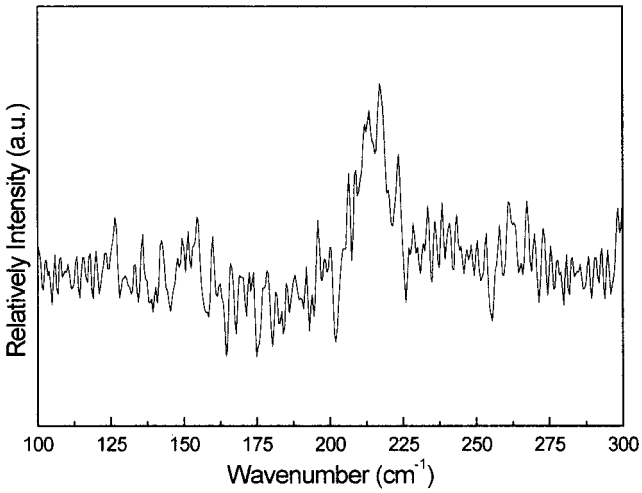

Figure 5. Raman spectrum of $NiSe_2$ at room temperature.

Preparation and Characterization of $CoSe_2$. The XRPD pattern of the product, which was obtained by replacing $NiCl_2$ with $CoCl_2$ in the similar reaction at 200 °C for 12 h, differed from those of the known cobalt selenide. However, no diffraction peaks belonging to oxides, selenates, or element were observed in the pattern. So, EDXA and XPS techniques were used to determine the composition of the product.

EDXA spectrum of the product revealed that only cobalt and selenium were present in the product. A quantitative EDXA analysis showed a molar ratio of Co:Se of 36.4:63.6, in reasonable agreement with the expected value of 33.3:66.6, although it indicates a slight excess of cobalt. EDXA data over several sites confirmed that the surface composition was uniform. No appreciable quantities of carbon or oxygen were observed over a number of surface sites.

However, since EDXA techniques cannot provide direct information as to the chemical nature of cobalt and selenium, XPS spectra of the product were measured, as shown in Figure 6. The typical survey spectrum of the product showed the presence of cobalt and selenium besides carbon and oxygen. The existence of carbon and oxygen was inevitable in the product exposed to air. The binding energies of Co 2p3 at 778.25 eV and Se 3d at 54.30 eV were consistent with the reported value of $CoSe_2$.[18] Meanwhile, a pronounced shake-up satellite was found at the higher energy side of the Co 2p3 signal, which can be attributed to the transition from metal the 3d to the ligand antibonding orbital.[24,25] Since shake-up satellites were found only in paramagnetic compounds, this result implied that the obtained $CoSe_2$ corresponded to a d^7 paramagnetic configuration.[26]

The comprehensive result of EDXA and XPS showed that the product could be identified as $CoSe_2$. It was interesting to note that the diffraction pattern of the

(21) Anastassakis, E. *Solid State Commun.* **1973**, *13*, 1297.
(22) Suzuki, T.; Uchinokura, K.; Sekine, T.; Matsuura, E. *Solid State Commun.* **1977**, *23*, 847;
(23) Lutz, H. D.; Himmirch, J.; Mueller, B.; Schneider, G. *J. Phys. Chem. Solid* **1992**, *53* (6), 815.
(24) Frost, D. C.; Ishitani, A.; McDowell, C. A. *Mol. Phys.* **1972**, *24*, 861.
(25) Vernon, G. A.; Stucky, G.; Carlson, T. A. *Inorg. Chem.* **1976**, *15*, 278.
(26) Matienzo, L. J.; Yin, L. I.; Grim, S. O.; Swarz, W., Jr. *Inorg. Chem.* **1973**, *12*, 2762.

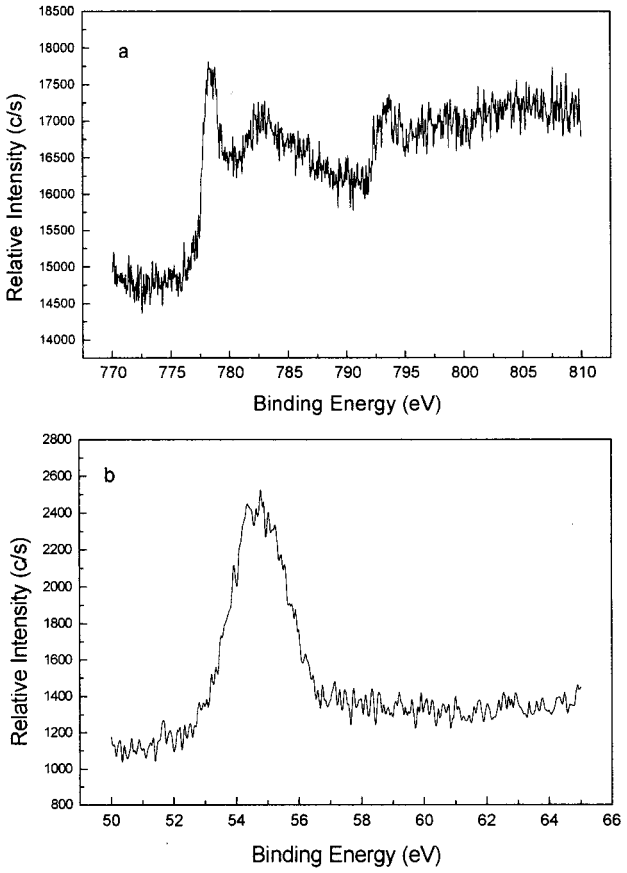

Figure 6. High-resolution region of (a) Co 2p3 and (b) Se 3d.

obtained $CoSe_2$ was very similar to that of $FeSe_2$(I).[27] Meanwhile, since many properties of VIIIB metals, such as ionic radius and electronegativity, are similar, it is probably that the obtained $CoSe_2$ has a structure similar to that of $FeSe_2$(I).

On the other hand, the XRPD pattern of the obtained $CoSe_2$ was closely related with that of $CoSe_2$ (Hastite).[28] All the diffraction peaks of Hastite in the literature were observed in the diffraction pattern of the obtained $CoSe_2$, but some diffraction peaks of the obtained $CoSe_2$ were not found in the diffraction pattern of Hastite. Furthermore, although Hastite belongs to orthorhombic system, the number of diffraction peaks in the literature is much less than expected. This indicates that the diffraction peaks of Hastite in the literature seems to be incomplete. To verify this conclusion, all the possible diffraction peaks of Hastite were worked out according to the known cell constants and crystal system. Through comparing these theoretical diffraction peaks with the observed ones of the obtained $CoSe_2$, it was found that the obtained $CoSe_2$ could be identified as the orthorhombic structure with the space group of *Pnnm*, which is the same as that of $FeSe_2$(I). The good conformity of the theoretical values with the observed ones demonstrated that the diffraction peaks of Hastite were incomplete, which is consistent with the aforementioned conclusion.

On the basis of this result, the diffraction pattern was indexed with the cell constants $a = 4.850$ Å, $b = 5.827$ Å, and $c = 3.628$ Å. The calculated diffraction peaks

(27) $FeSe_2$(I), JCPDS Card, No. 12-291.
(28) $CoSe_2$(Hastite), JCPDS Card, No. 10-408.

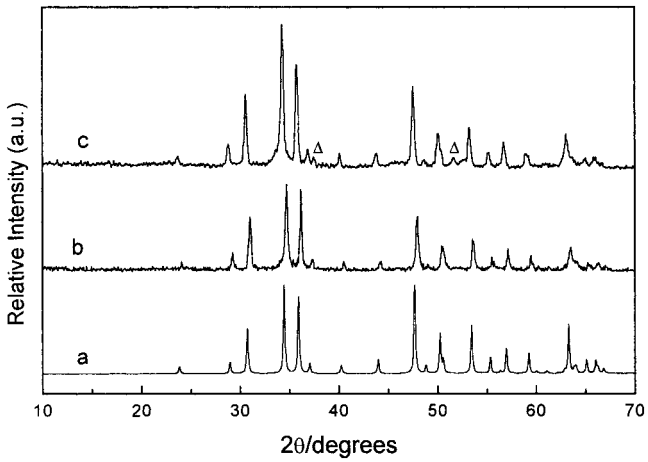

Figure 7. (a) Calculated XRPD pattern of $CoSe_2$ (Hastite); (b) the XRPD pattern of the obtained $CoSe_2$ (Hastite) prepared at 200 °C for 12 h; (c) the XRPD pattern of $CoSe_2$ prepared at 170 °C for 12 h, $CoSe_2$ (Hastite) + $CoSe_2$ (Trogtalite, △)

Table 2. Calculated Values of $CoSe_2$ and the Observed Values of $CoSe_2$

·*h k l*⟩	2θ	*d*-value (calcd)	I/I_0, % (calcd)	*d*-value (obsd)	I/I_0, % (obsd)
110	23.851	3.7277	7.7	3.7292	8.5
011	28.968	3.0798	13.1	3.0792	18.6
020	30.661	2.9135	5.9		
101	30.752	2.9051	47.2	2.9029	53.3
111	34.468	2.5999	100	2.5959	100
120	35.929	2.4975	86.7	2.4953	89.9
200	37.042	2.4250	11.2	2.4257	13.6
210	40.249	2.2389	9.2	2.2315	9.5
121	43.980	2.0572	15.7	2.0581	13.1
211	47.694	1.9053	100	1.9041	64.8
220	48.822	1.8639	9	1.8661	9.5
002	50.256	1.8140	44.8	1.8149	34.7
130	50.581	1.8031	14.6	1.8005	16.8
031	53.467	1.7124	54.2	1.7119	37.7
221	55.373	1.6579	18.2	1.6564	14.6
112	56.361	1.6311	2.7		
131	56.987	1.6147	28.2	1.6156	25.6
310	59.270	1.5578	23.1	1.5578	11.1
022	60.029	1.5399	2.8	1.5422	6.0
230	61.077	1.5160	3	1.5148	5.5
301	62.884	1.4767	3.3	1.4754	6.0
122	63.314	1.4677	55.3	1.4681	27.6
040	63.846	1.4568	6	1.4547	14.1
202	64.052	1.4526	8	1.4514	6.8
311	65.113	1.4314	15.7	1.4320	11.6
320	66.037	1.4136	14.3	1.4101	11.1
212	66.259	1.4094	6.6	1.4097	5.3
231	66.829	1.3988	5.6	1.3967	4.8
140	67.025	1.3952	0.4		

based on this set of the cell constants were in good agreement with the observed ones, which is shown in Figure 7. The indexed results are summarized in Table 2. When observed by electron microscope, the product prepared at 200 °C for 12 h was composed of nanoparticles and a small amount of nanorods.

According to the result of $NiSe_2$, that nanorods were prone to appearing in the product at low temperature, the same reaction was conducted at 170 °C. The obtained product was mainly composed of nanorods. A typical $CoSe_2$ nanorod 440 nm in length and 120 nm in width was shown in Figure 8a. Its SAED pattern (Figure 8b) showed that it was a well-developed single crystal with its growth direction along ⟨121⟩ . Meanwhile, a trace of cubic phase $CoSe_2$ was also found in the product, because its characteristic diffraction peaks

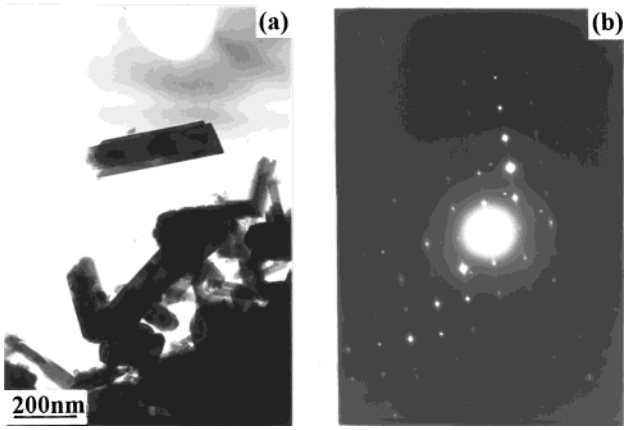

Figure 8. TEM and SAED photographs of $CoSe_2$ prepared at 170 °C for 12 h.

with the *d*-values at 2.389 and 1.765 Å appeared in the pattern with lower intensity by contrast to other diffraction peaks.[29]

TG analysis of $CoSe_2$ revealed a similar process to that of $NiSe_2$. The thermal decomposition with its onset at 546.32 °C and its end at 625.47 °C gradually lost weight to about 63.47%, which was close to the theoretical value of 63.34%. The final product was identified as Co_3O_4 by the XRPD technique. According to the results, the molar ratio of Co:Se was calculated to be 1:2.01.

Preparation and Characterization of $FeSe_2$. When a similar reaction was used to prepare $FeSe_2$, the obtained product was washed with a diluted HCl solution to remove iron oxides. The product at 120 °C consisted of crystalline Se and $FeSe_2$, as shown in Figure 9a. If the temperature was increased up to 160 °C, the product was identified as a mixture of two different $FeSe_2$ phases (Figure 9b). Although most of the diffraction peaks of both phases are identical, the characteristic diffraction peaks of $FeSe_2$(I) at 3.73 Å and that of $FeSe_2$(II) at 3.69 Å were observed in the diffraction pattern.[27,30] When the reaction was conducted at 180 °C, only $FeSe_2$(I) was observed in the product (Figure 9c). The TEM photograph revealed that it was irregular nanoparticles in the range 40−100 nm.

Conclusion

In summary, transition metal diselenides (MSe_2, M=Ni, Co, Fe) were prepared via a solvothermal reduction route at low temperatures. The compositions of these diselenides were identified by EDXA and XPS techniques. The various shapes of $NiSe_2$, such as filaments, irregular particles, and octahedra, were observed and were well controlled by changing the synthetic conditions. TG-DTG analysis showed that NiSe played an intermediate role in the pyrolysis process of $NiSe_2$. The whole process was that $NiSe_2$ pyrolyzed to produce NiSe, which then was oxidized to NiO. The intraionic Se−Se stretching mode at 216.5 cm^{-1} was observed in the Raman spectrum of $NiSe_2$. The XRPD pattern of $CoSe_2$ nanoparticles was indexed as the orthorhombic structure similar to that of $FeSe_2$. At low temperature there was a trace of the cubic phase $CoSe_2$ in the product besides the orthorhombic phase $CoSe_2$. TEM and SAED revealed that this product was composed of nanorods with the growth direction along ⟨121⟩ . Two similar Ferroselite phases and the transition between them were observed in the product.

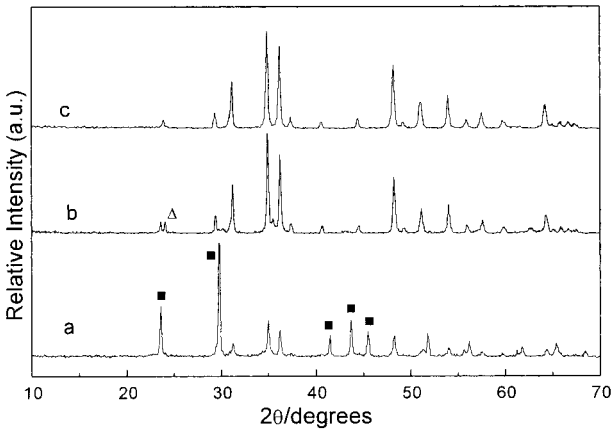

Figure 9. XRPD pattern of $FeSe_2$ prepared at different temperature for 12 h: (a) 120 °C, $FeSe_2$(I) +Se(■); (b)160 °C, $FeSe_2$(I) + $FeSe_2$ (II,△); (c) 180 °C, $FeSe_2$(I).

Acknowledgment. This research is supported by the Chinese Natural Science Research, Anhui Provincial Foundation of Natural Science Research, and National Climbing Program. We gratefully thank Associate Prof. W. Q. Zhang for manipulating the X-ray diffractometer, Prof. G. E. Zhou, and Prof. L. B. Wang for beneficial discussions.

CM0005945

(29) $CoSe_2$(Trogtalite), JCPDS Card, No. 9-234.
(30) $FeSe_2$(II), JCPDS File, No. 21-432.